

Heat Exchanger Design for Thermoelectric Electricity Generation
from Low Temperature Flue Gas Streams

by

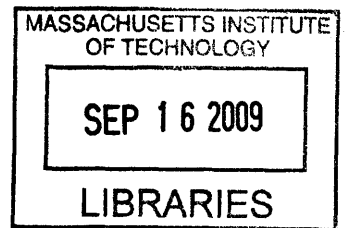
Jacob G. Latcham

SUBMITTED TO THE DEPARTMENT OF MECHANICAL ENGINEERING IN
PARTIAL FULFILLMENT OF THE REQUIREMENTS FOR THE DEGREE OF

BACHELOR OF SCIENCE
AT THE
MASSACHUSETTS INSTITUTE OF TECHNOLOGY

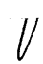
JUNE 2009


© 2009 Jacob G. Latcham. All rights reserved.




The author hereby grants to MIT permission to reproduce
and to distribute publicly paper and electronic
copies of this thesis document in whole or in part
in any medium now known or hereafter created.

ARCHIVES

Signature of Author..... 
Department of Mechanical Engineering
May 11th, 2009

Certified by..... 
Gang Chen
Warren and Towneley Rohsenow Professor of Mechanical Engineering
Thesis Supervisor

Accepted by..... 
John H. Lienhard V
Collins Professor of Mechanical Engineering
Chairman, Undergraduate Thesis Committee

Heat Exchanger Design for Thermoelectric Electricity Generation
from Low Temperature Flue Gas Streams

By

Jacob G. Latcham

Submitted to the Department of Mechanical Engineering
on May 8, 2009 in partial fulfillment of the
requirements for the Degree of Bachelor of Science in
Mechanical Engineering

ABSTRACT

An air-to-oil heat exchanger was modeled and optimized for use in a system utilizing a thermoelectric generator to convert low grade waste heat in flue gas streams to electricity. The NTU-effectiveness method, exergy, and thermoelectric relations were used to guide the modeling process. The complete system design was optimized for cost using the net present value method. A number of finned-tube compact heat exchanger designs were evaluated for high heat transfer and low pressure loss. Heat exchanger designs were found to favor either power density or exergy effectiveness to achieve optimal net present value under different conditions. The model proved capable of generating complete thermoelectric flue gas systems with positive net present values using thermoelectric material with a ZT value of 0.8 and second law efficiency of 13%. Complete systems were generated for a number of economic conditions. The best complete system achieved a first law efficiency of 1.62% from a 150° C flue gas stream at an installed cost of \$0.79 per watt.

Thesis Supervisor: Gang Chen

Title: Warren and Townley Rohsenow Professor of Mechanical Engineering

Table of Contents

| | |
|--|-----------|
| 1. Introduction..... | 4 |
| 1.1 Uses of Flue Gas Waste Heat..... | 5 |
| 1.2 Comparison of TEGs to Traditional Heat Engines..... | 5 |
| 2. TEG System Design..... | 7 |
| 2.1 Air to Oil Heat Exchanger..... | 8 |
| 2.2 Oil to TEG Heat Exchanger | 8 |
| 2.3 Net Present Value..... | 9 |
| 3. System Modeling and Optimization..... | 10 |
| 3.1 Fin Type Study | 10 |
| 3.2 Effectiveness-NTU..... | 11 |
| 3.3 Pressure Drop and Power Calculations..... | 13 |
| 3.4 Exergy Calculations..... | 14 |
| 3.5 Cost Calculations..... | 16 |
| 3.6 Optimization Strategy..... | 17 |
| 4. Results..... | 19 |
| 4.1 Fin Selection..... | 19 |
| 4.2 Heat Exchanger..... | 20 |
| 5. Discussion..... | 26 |
| Acknowledgements..... | 30 |
| Appendix A..... | 31 |
| References..... | 33 |

1. Introduction

Non-renewable electricity generation and a number of manufacturing processes reject large quantities of energy into the atmosphere each year in the form of waste heat. According to the United States Department of Energy, over 100 GWyrs of energy are wasted each year from manufacturing processes alone. This waste heat comes from process inefficiencies and is typically unrecoverable using conventional technologies because of the relatively low temperatures (usually below 400° Fahrenheit or 200°C) that the heat is rejected at. This large volume of low grade waste heat presents significant opportunity for new and more effective energy recovery technologies to capture interest and market share, especially as energy prices climb and concern over climate change affects regulatory policy on process efficiencies.

One potential option for the converting low grade waste heat into electricity is to use a thermoelectric generator, or TEG. A TEG is a solid state device that converts heat into electricity by the Seebeck effect¹. TEGs have recently emerged as viable electricity generators because of improved thermodynamic efficiencies and higher survivable operating temperatures¹.

In this thesis the economic feasibility of a TEG low grade waste heat recovery system is explored in greater detail via the optimization of a hypothetical system installed downstream of a gas turbine combined-cycle power plant. The flue to oil heat exchanger is modeled using the NTU method. The overall system is modeled with an exergy balance. The waste heat system is optimized for cost using traditional heat transfer and thermoelectric material relations, the net present value method for evaluating capital projects, and costs gathered from industry in order to realistically evaluate the profitability of such a system.

1.1 Uses of Flue Gas Waste Heat

Low grade waste heat can be used for a number of processes, and common uses include preheating combustion gases, heating and cooling buildings, and providing heat to industrial reactions or manufacturing processes¹. Typically recycling waste heat for processes is more valuable than producing electricity, but recycling can require significant infrastructure changes and in many cases simply is not practical. Electricity production from waste heat, on the other hand, is a stand alone process that produces a universally tradable commodity. Thus, electricity production is smart alternative when process recycling cannot be implemented. Organic Rankine cycles (ORC), Stirling cycles, or other thermodynamic engines, such as a TEG, can be used to convert waste heat into electricity.

1.2 Comparison of TEGs to Traditional Heat Engines

There are a number of advantages to TEGs which make them particularly attractive for use in waste heat conversion to electricity. Scalability, low maintenance, and ability for use with low temperature streams are the most significant. Current short-term limitations include moderate conversion efficiency, high cost, and lack of field testing.

A TEG system is easily scaled to optimally match the size of its waste heat source without major redesign; a 10 MW heat source will require roughly 20 times the number of TEG units required for a 500 kW source. Such linear scalability is not possible with traditional heat engines; either multiple engines must be used (meaning more maintenance) or a new engine must be designed. Additionally, traditional heat engines are designed to operate in a specific range of temperatures and flowrates, which means they may operate outside of their thermodynamic optimum in a real application. This study will show that TEGs can be

applied to a large range of operating temperatures with little to no change in the design of the system.

Maintenance is also an area where TEG systems outperform heat engines. Since TEGs have no moving parts and are modular, they require less preventative maintenance and are simpler to repair. Heat engines are susceptible to a number of mechanical failures, due to the forces and pressures exerted on them during continuous use, and since most are not modular, repair can take an entire system offline. Stirling engines are historically notorious for Heat engines have additional complexity in that they must interface with an electromechanical transducer in order to produce electricity.

TEGs are not as constrained by temperature as an ORC because they are not dependent on a phase-changing working fluid. Thus, while most commercial ORC waste heat systems require inlet temperatures between 400° and 500° Fahrenheit to even operate^{2,3}, bismuth telluride TEGs scale linearly with Carnot efficiency from room temperature to 390° Fahrenheit⁴.

TEGs cannot match the organic Rankine cycle in terms of first law efficiency. Typical ORCs operate between 5% and 12% efficiency³, whereas current TEG systems peak at efficiencies near 5%⁴. This may be primarily because ORC is a mature technology and is available commercially. Companies like Turboden s.r.l. in Italy produce large scale ORC systems generating 500 kW to 2 MW, while companies like Electratherm, Inc focus on smaller 50 to 500 kW systems. However, both are dependent on flue gas streams hotter than 400° Fahrenheit to operate, leaving flue gas streams in the 300° Fahrenheit range unusable, a temperature at which the DOE estimates 40 GWyrs of energy is released per year.

2. TEG System Design

Initially designs for the study focused on a system for real world testing at MIT's cogeneration plant. However, final designs were freed of mass flow constraints to develop systems deployable in any size clean flue gas stream. Streams of particular interest were those from natural gas combustion, which are mostly free of particulate matter and sulfur compounds. The system employs an air to liquid heat exchanger in the flue gas exhaust stream to heat a thermal oil stream. The thermal oil is then transferred to a TEG stack, where the heat from the thermal oil is transferred to one surface of the TEG. Water is used to cool the opposite side of the TEG to create a temperature differential across the TEG and generate a voltage. The DC electricity produced by the TEG is then passed to a DC to AC converter, of which this paper is not concerned, where it can be fed into the facilities grid or used on site. A schematic of the process is illustrated on the following page in Figure 1.

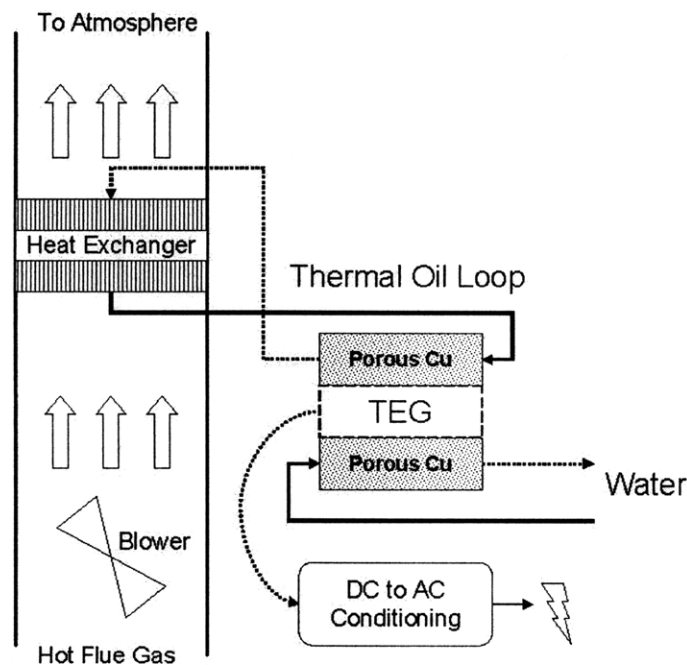


Figure 1: Hot flue gas is used to heat thermal oil via a finned tube heat exchanger. The hot thermal oil is then passed through a porous copper heat exchanger on one side of a TEG unit while cool water is passed through another porous copper heat exchanger on the opposite side of the TEG. The DC voltage produced by the TEG is then converted to AC and distributed.

2.1 Air to Oil Heat Exchanger

Recovering heat from gaseous fluid streams is capital intensive due to the large heat exchanging surfaces required. Gases generally have lower heat capacities and lower convection coefficients when compared to similarly dimensioned liquid streams. Therefore gases generally require compact, highly-finned heat exchangers to adequately transfer heat to another fluid stream⁵. Such configurations have inherently small hydraulic diameters, resulting in high friction factors and high pressure drops. Heat exchanger design for gaseous fluid streams then must pay special attention to the pumping power required for a certain geometry and set of operating conditions⁶.

In the case of the TEG system, it is critical that the pumping power required by the flue gas blower is smaller than the power produced by the TEG, or the system would have no value. As such, several flow arrangements and heat exchanger types were explored. Transferring the flue gas heat directly to the TEG was considered, but low heat transfer rates and a complicated interface between the fins and TEG, along with maintenance and stress issues, created the need for an intermediate fluid. High temperature thermal oil was chosen to shuttle heat from the flue gas stream to the TEG stack to avoid two-phase flow and to maximize the temperature captured, as well as to avoid internal heat transfer surface fouling. Direct contact heat exchangers were also considered, but current commercial designs fail to reach temperatures acceptable for effective TEG use.

2.2 Oil to TEG Heat Exchanger

The oil to TEG heat exchanger stack is an area of ongoing design work and was not modeled in this study. MIT graduate student Andrew Muto, of Prof. Gang Chen's laboratory, was investigating configurations of plate-fin and porous copper heat exchangers for use in

such a system at the time of the submittal of this paper. The power losses due to the high pressure drop required to pass thermal oil through porous copper, or a plate-fin heat exchanger, were assumed negligible relative to the power consumed by the air to oil heat exchanger. This assumption will be tested in the future for validity.

2.3 Net Present Value

Capital building projects undertaken by industry are often evaluated on a of cost basis to determine if the project should or should not be financed. Typical evaluation methods include calculating the project's payback period, internal rate of return, or net present value. Of these three methods, only net present value provides a consistent basis for comparison of projects and definite answers to when a project should be undertaken, and as such it was the method used to compare and optimize the TEG system designs⁷. The net present value (NPV) method accounts for all costs and incomes during the life of a project and discounts each year's cash flows using a discount rate chosen by the projects financiers. If two or more projects are being compared, the project with the highest positive NPV should be built, as it will add value to the company's bottom line⁷. The payback period method ignores revenue after the project has been paid off and also fails to discount cash flows. These two shortcomings can prevent a firm from undertaking value adding projects. Internal rate of return also prevents firms from undertaking valuable projects if their chosen internal rate of return is too high or a project's discounted cash flows sum to zero. For a more detailed discussion the author recommends reading Brealey, Myers and Allen's *Principles of Corporate Finance*.

3. System Modeling and Optimization

The system was modeled such that it could be optimized to produce the highest installed net present value on a per TEG watt basis. A number of finned tube designs were explored. The system was modeled in MatLab; the NTU method was used to model the air to oil heat exchanger, and an exergy balance and power density were used to evaluate the system.

3.1 Fin Type Study

Selection of an efficient air to oil heat transfer surface was of critical importance to maximizing the exergy recovered from the flue gas. Kays and London suggest comparing finned tube surfaces on a power per unit area and heat transfer per unit area basis when exergy recovery is of importance. One can specify fluid properties, along with Reynolds number and the friction factor of a surface, to determine the power consumed by a unit of surface using the equation

$$E = \frac{1}{2g_c} \frac{\mu^3}{\rho^2} \left(\frac{1}{4r_h} \right)^3 f \text{Re}^3, \quad [1]$$

which depends on a second law proportionality factor, g_c , the fluid viscosity, μ , the fluid density, ρ , the hydraulic diameter of the finned surface, $4r_h$, and the friction factor and Reynolds number. To determine the heat transfer per unit of surface area for a finned surface, Kays and London provide the equation

$$h = \frac{c_p \mu}{\text{Pr}^{2/3}} \frac{1}{4r_h} (j^{2/3}) \text{Re}, \quad [2]$$

which is calculated using the Prandtl number of the fluid, Pr , the heat capacity, c_p , and the Colburn factor of the surface, j , along with several variables shared with Equation 1.

Plotting h versus E allows different finned tube surfaces to be compared on an equal basis. Kays and London provide both j and f as functions of Reynolds number for a number of commercially available surfaces.

3.2 Effectiveness – NTU Calculations

The NTU-effectiveness method was employed to size the air to oil heat exchanger. An array of oil inlet temperatures, flue gas Reynolds numbers, NTU values, and oil flowrate to flue gas flowrate ratios were used to define other parameters. The first step in the sequence involved calculating the heat exchanger effectiveness for a given set of conditions. The overall oil flow arrangement was modeled as purely counter-flow, however in a real system the oil flow arrangement would be a hybrid of cross-flow and counter-flow. The counter-flow effectiveness relation is defined as

$$\varepsilon = \frac{1 - \exp(-NTU(1 - C^*))}{1 - C^* \exp(-NTU(1 - C^*))} \quad [3]$$

The variable C^* is the ratio of the heat capacity flowrate of the oil stream to that of the air stream. The effectiveness can be used, along with the specified oil and flue gas inlet temperatures, to find the inlet and outlet temperatures of the flue and oil. The oil outlet temperature is

$$T_{oil,o} = T_{oil,i} + \varepsilon(T_{flue,i} - T_{oil,i}), \quad [4]$$

while the flue gas outlet temperature is given by

$$T_{flue,o} = T_{flue,i} - C^*(T_{oil,o} - T_{oil,i}). \quad [5]$$

The next group of calculations focused on determining the overall heat transfer coefficient per unit area of the heat exchanger. The coefficient is a sum of the air side convection coefficient,

conduction resistance through the finned tube, and the oil side convection coefficient. The inverse of the overall transfer coefficient per unit air-side area is

$$\frac{1}{U} = \frac{1}{h_{oil} A_{oil} / A_{flue}} + A_{flue} R_w + \frac{1}{\eta_{fin} h_{flue}} \quad [6]$$

where R_w is the tubing resistance to conduction and η_{fin} is the fin efficiency.

The flue gas convection coefficient is calculated first by finding the maximum mass flowrate for the chosen surface, G , using the flue gas physical properties and the hydraulic diameter of the fin surface, D_h .

$$G = \frac{Re \mu}{D_h} \quad [7]$$

Equation 7 gives the maximum mass flowrate through a single channel in the heat exchanger matrix. G and the Colburn factor, j , which is a function of surface geometry and Reynolds number, are together used to determine h_{flue} :

$$h_{flue} = \frac{j G c_{p,air}}{Pr^{2/3}} \quad [8]$$

The tubing wall conduction resistance, $A_h R_w$, is calculated using an equation from Incropera.

$$A_h R_w = \frac{D_i \ln(D_o / D_i)}{2k(A_{oil} / A_{flue})} \quad [9]$$

The inner and outer diameters are given by D_i and D_o , while k is the conductivity of the tubing material and A_{oil} and A_{flue} produce a ratio of oil heat transfer area to air heat transfer area.

The oil convection coefficient was assumed to be large enough to drive its contribution to the overall transfer coefficient to zero. Additionally, the complexity of liquid flow arrangements in compact finned tube heat exchangers made modeling a realistic route and flowrate for the oil difficult.

With the overall transfer coefficient in hand and the NTU specified, the depth of the heat exchanger can be calculated by rearranging the typical NTU relation to:

$$L = \frac{NTU c_{p,air} C^* G}{U \alpha}, \quad [10]$$

where $c_{p,air}$ is the heat capacity of air at the operating conditions and α is the heat transfer area to volume ratio of the particular finned tube surface. L is used to calculate the pressure drop across the heat exchanger, and it also signals when the model generates an unrealistically thin heat exchanger.

3.3 Pressure Drop and Power Calculations

The pressure drop across the exchanger is broken down into entrance effects and bulk effects. The entrance effect drop, due to the acceleration and deceleration of the gas, is found using the equation below:

$$\Delta p_{entrance} = \frac{G^2 v_i}{2} \left(1 + \sigma^2 \left(\frac{v_o}{v_i} - 1\right)^5\right). \quad [11]$$

In Equation 11, σ is the ratio of the free-flow area to the frontal area for the specific finned tube surface being used. The values of v are the inlet and outlet specific volumes of the flue gas, which is approximated as air. The bulk pressure drop is a function of the finned tube's friction factor, and is defined as

$$\Delta p_{bulk} = \frac{f G^2}{2 \rho_{flue} \frac{L}{D_h}}. \quad [12]$$

The pressure drops are summed together to form Δp_{net} , which can then be used to calculate the power consumed by the flue gas blower at a specified flue gas to oil flowrate.

$$\dot{W}_{blower} = \frac{\Delta p_{net}}{\eta_{blower} \rho_{flue} C_{p,air}} \quad [13]$$

The term in the denominator is the efficiency of the blower, which was assumed to be 0.8 to represent most industrial blowers.

3.4 Exergy Calculations

One of the critical optimization steps for air to oil heat exchanger was maximizing the exergy in the hot oil stream. This was done by maximizing a ratio of exergy in the hot oil stream to total exergy in the flue gas stream. The exergy rate of the air stream, neglecting the phase change of water vapor and other species, was defined as:

$$\dot{\Lambda}_{flue} = C_{flue} (T_{flue,hot} - T_{\infty}) - C_{flue} T_{\infty} \ln \left(\frac{T_{flue,hot}}{T_{\infty}} \right). \quad [14]$$

In Equation 14, C_{flue} is the heat capacity flowrate of the flue gas stream, while $T_{flue,hot}$ is the exhaust temperature of the flue gas, and T_{∞} is the temperature of the cooling water used on the TEG cold side. The exergy rate in the oil stream is then similarly defined as

$$\dot{\Lambda}_{oil} = C_{oil} (T_{oil,hot} - T_{oil,cold}) - C_{oil} T_{\infty} \ln \left(\frac{T_{oil,hot}}{T_{oil,cold}} \right) - C_{flue} \dot{W}_{pump}. \quad [15]$$

The pumping power is the sum of the power required to pump the oil through the heat exchanger and the power used by the flue gas blower overcome the pressure drop across the heat exchanger's finned tube banks. Pumping compressible gases is significantly more energy intensive than pumping liquids, so it was assumed that the power required to pump thermal oil was negligible. Stacking the two exergy flow rate terms, we get:

$$\frac{\dot{\Lambda}_{oil}}{\dot{\Lambda}_{flue}} = \frac{C_{oil}(T_{oil,hot} - T_{oil,cold}) - C_{oil}T_{\infty} \ln\left(\frac{T_{oil,hot}}{T_{oil,cold}}\right) - \frac{C_{flue}\dot{W}_{blower}}{\eta_{TE,II}}}{C_{flue}(T_{flue,hot} - T_{\infty}) - C_{flue}T_{\infty} \ln\left(\frac{T_{flue,hot}}{T_{\infty}}\right)}. \quad [16]$$

In Equation 16, $\eta_{TE,II}$ is the second law efficiency of the thermoelectric material. This efficiency is calculated using the thermoelectric material's non-dimensional figure of merit, ZT. ZT is generally assumed constant over small ranges of temperatures⁴.

$$\eta_{TE,II} = \frac{\sqrt{Z\bar{T} + 1} - 1}{\sqrt{Z\bar{T} + 1} - \frac{T_{\infty}}{T_H}} \quad [17]$$

In Equation 17, T_{∞} and T_H are the cold and hot temperatures on either side of the thermoelectric. Returning to the exergy ratio, we can consolidate the mass heat capacity terms by defining C^* as the ratio of C_{oil} to C_{flue} . We can then substitute C^* into the exergy ratio to get:

$$\frac{\dot{\Lambda}_{oil}}{\dot{\Lambda}_{flue}} = \frac{C^* \left(T_{oil,hot} - T_{oil,cold} - T_{\infty} \ln\left(\frac{T_{oil,hot}}{T_{oil,cold}}\right) \right) - \frac{\dot{W}_{blower}}{\eta_{TE,II}}}{(T_{flue,hot} - T_{\infty}) - T_{\infty} \ln\left(\frac{T_{flue,hot}}{T_{\infty}}\right)}. \quad [18]$$

With the exergy ratio in hand, the first law efficiency of the entire system can be calculated using:

$$\eta_{system,I} = \frac{\eta_{TE,II} \dot{\Lambda}_{oil}}{C_{flue} \Delta T} = \frac{\eta_{TE,II} \dot{\Lambda}_{oil}}{\dot{\Lambda}_{flue} / \eta_C} = \frac{\dot{\Lambda}_{oil}}{\dot{\Lambda}_{flue}} \eta_{TE,II} \frac{1 - T_{\infty} \ln\left(\frac{T_{flue,hot}}{T_{\infty}}\right)}{T_{flue,hot} - T_{\infty}}, \quad [19]$$

where again $\eta_{TE,II}$ is the second law efficiency of the thermoelectric material, and the third group of terms calculates the Carnot efficiency of the system.

With the heat exchanger temperatures, relative flowrate, and blower power defined, the power recovered from the flue gas by the heat exchanger can be calculated on a unit volume basis, and will henceforth be referred to as the “power density”:

$$P_{density} = \frac{Power_{TE}}{Volume_{HEX}} = \frac{C^* \eta_C \eta_{TE,II} - \dot{W}_{blower}}{\frac{L}{Gc_{p,air}}} \quad [20]$$

$$= \frac{Gc_{p,air}}{L} \left(\eta_{TE,II} C^* \left(T_{oil,o} - T_{oil,i} \right) - T_{\infty} \ln \left(\frac{T_{oil,o}}{T_{oil,i}} \right) \right) - \dot{W}_{blower}$$

The power density and exergy ratio provide physical parameters that allow for evaluation of different heat exchanger designs and operating conditions.

3.5 Cost Calculations

The NPV of a system was calculated using the exergy ratio, power density, and set of fluid temperatures calculated using the equations above. Economic data gathered from industry allowed for realistic estimations of costs.

The system costs were simplified and modeled as consisting of the cost of the manufactured TEG material, the cost of the manufactured air to oil heat exchanger, the cost of the installation of the heat exchanger, and the operating costs for yearly maintenance of the system.

The TEG cost was calculated on a per watt basis and was dependent on the inlet and outlet oil temperatures and the cooling water temperature⁴.

$$Cost_{TEG} = \left(\frac{\$_{TE}}{kg} \right) \cdot \rho_{BiTe} \cdot \frac{4l^2}{ZT \cdot k} \cdot \left(\frac{2}{0.8(T_{oil,i} + T_{oil,o} - 2T_{\infty})} \right)^2 \quad [21]$$

The first term to the right of the equal sign in Equation 21 is the cost of TE material in dollars per kilogram, which is then multiplied by the density of bismuth telluride to get a cost per volume of TE. The third term uses the properties of the TE to determine the volume of TE material required for one watt of power, with l being the thickness of the TEG, ZT being the figure of merit for the TE material, and k being the conductivity of the thermoelectric material. The final term calculates the average temperature differential across the TEG and scales it based on the thermal resistances of the TE material.

The cost of the heat exchanger and its installation were found empirically by designing several systems and gathering quotes from heat exchanger manufacturers. The overall initial cost per watt of the TEG system is then defined as:

$$Cost_{System} = \frac{Cost_{Hex}}{P_{density}} + Cost_{TEG} \cdot \quad [22]$$

The NPV of a project is the summation of yearly net cash flows discounted to their present day value, with r being the firm's discount rate; the number of cashflows equals the number of years the system is operational:

$$NPV = CF_o + \frac{CF_1}{(1+r)} + \frac{CF_2}{(1+r)^2} + \dots \quad [23]$$

Cash outflows for the system are the initial cost of the system in year one, yearly taxes, and yearly operating costs, which were assumed to be constant and 5% of the initial cost of the system. Cash inflows were the result of selling electricity produced by the system. The net cash flow in the first year is negative and equal to the cost of the entire system. Net cash flows in all years following the first are equal to

$$\begin{aligned}
CF_0 &= Cost_{system}, \\
CF_{1 \rightarrow n} &= CF_{electricity} - CF_{operating} - \tau(CF_{operating} - Depreciation)
\end{aligned}
\tag{24}$$

In the above equation, τ is the tax rate imposed on the firm (assumed to be 35%), and depreciation is the yearly linear depreciation of the initial system cost. The electricity cash flow comes from generating and selling one watt of electricity per year. In the model, an operating capacity term is used to calculate the electricity cash flow to account for system downtime. An operating capacity of 0.85 was assumed since the system is of low complexity.

The resulting NPV summation gives the value of one watt of installed system in today's dollars.

3.6 Optimization Strategy

The strategy for optimizing the design of the system was simple but computationally intensive. A MatLab script runs through thousands of combinations of inlet oil temperatures, flowrate ratios, Reynolds numbers, and NTU values. Support variables are calculated at each combination point, including the exergy ratio, power density, and NPV. The initial NPV value is stored, and if a subsequent NPV value exceeds the value of the previously stored NPV, then it becomes the new stored optimal value.

The NPV, as calculated in Equations 21-24, is on a per watt basis. If optimized solely for NPV per watt, the resulting system could be yield a high NPV but a particularly inefficient and small system that generates a low overall volume of electricity. To solve this problem, the NPV per watt was multiplied by the exergy ratio to positively weight systems which produce high volumes of electricity. All configurations were optimized for highest product of NPV and exergy ratio.

The MatLab code used for the simulation is available on request from members of Professor Gang Chen's laboratory.

4. Results

A number of finned-tube heat exchanger designs were compared, and the chosen surface was incorporated into the heat exchanger model. The model was then used to evaluate the effects of several economic parameters on the design of the system.

4.1 Fin Selection

Twenty-one fin configurations, including spiraled fin, contiguous fin, and flat tube designs were compared using the method described in section 3.1 and with properties of air at an operating temperature of 450 K. All surfaces and their parameters were taken from Kays and London and represent common, commercially available designs. Dimensions for each surface can be found in the appendix A. The figure on the next page plots the best performing surfaces from five surface sub-groups.

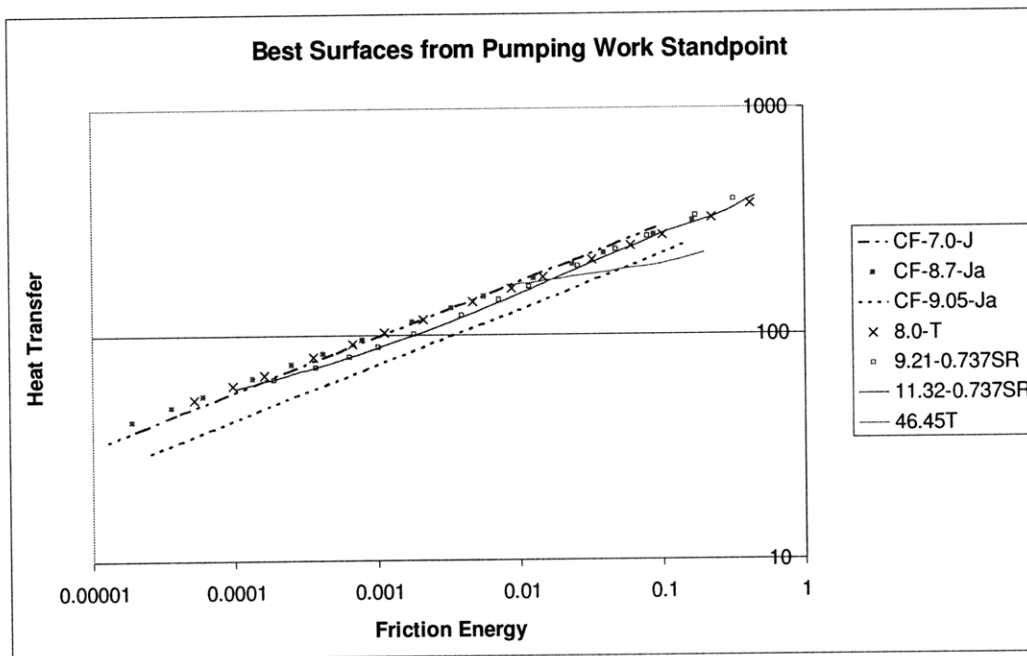


Figure 2: Heat transfer per unit area as a function of energy expended due to pressure loss per unit area for several finned tube heat exchanger designs. Surface 8.0-T was used in the main model.

Surfaces with a higher heat transfer rate at a given friction energy are more efficient at pulling energy out of an air stream. Surface 8.0-T, a continuous finned-tube surface, was selected for use in the modeled system because of its high relative performance and its manufacturing simplicity. Dimensions of the surface, along with values for the friction factor and Colburn factor, can be found in appendix A. Several manufactures were contacted and asked to price the surface on a unit volume basis, and the cost per cubic meter installed averaged \$7500/m³.

4.2 Heat Exchanger

Many of the economic parameters in the system are unknown to great certainty. As such, the optimizations performed focused on determining the influence of parameters such as system lifespan, discount rate, operating cost rate, and sale price of electricity.

The system parameters were optimized to yield the configuration with the highest NPV. For all cases the inlet air temperature was 150° C, unless otherwise noted, and all flue gas properties were for air at 150° C. The cooling water temperature, referred to as T_{∞} , was fixed at 21.85° C (295 K). The ZT value for all cases was 0.8, and the thermoelectric second law efficiency, $\eta_{TE,II}$, was held constant at 0.13.

A plot of heat exchanger power density as a function of exergy ratio was generated during each optimization case. Reynolds number ranged from 500 to 1500 in steps of 50, C^* from 0.05 to 0.95 in steps of 0.05, $T_{oil,in}$ from 40 to 140°C in steps of 5, and NTU from 0.1 to 7 in steps of 0.5. The plot can be found in Figure 3 on the next page.

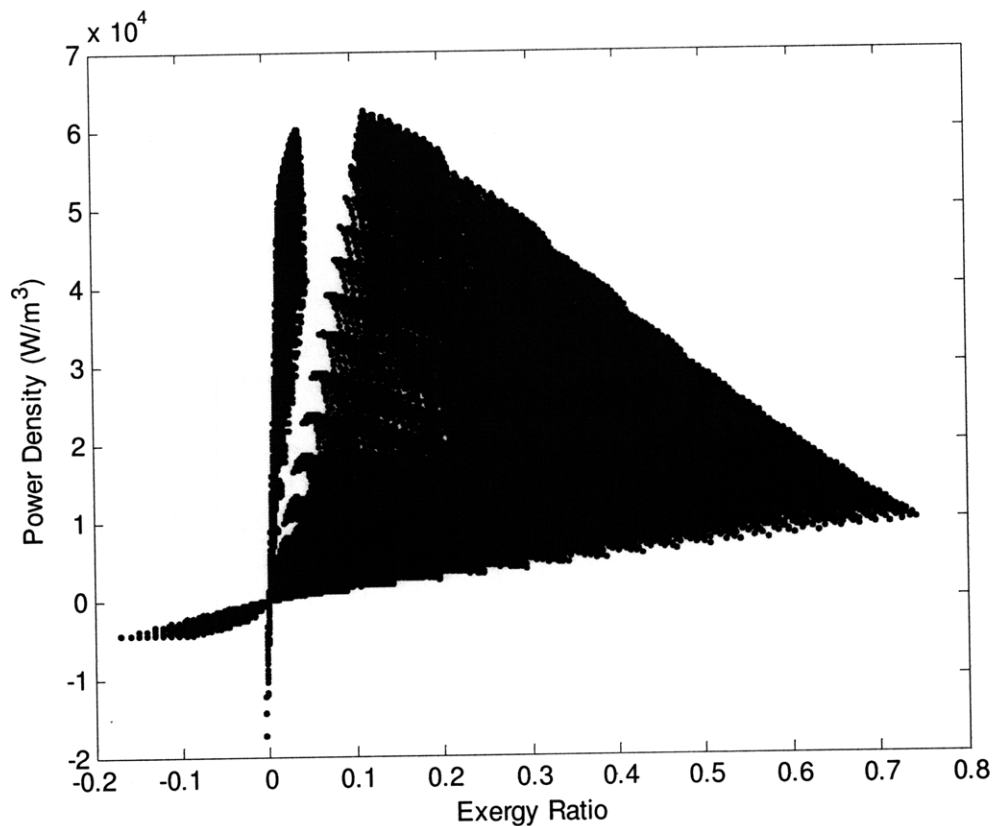


Figure 3: Power density as a function of exergy ratio for all values spanned during model optimization.

Table 1, below, details the results of systems optimized for lifetimes of 5, 10, and 15 years. Since no system has been built or field tested, the lifetime of the system is a significant unknown. The discount rate was 0.1, the operating cost rate was 0.05, and the price of electricity was \$0.10 per kW-hr.

| System Lifespan | Oil Inlet Temperature | Flue Gas Reynolds Number | Heat Exchanger Depth, L | First Law Efficiency | TE Cost | Hex Cost | Overall Cost | Weighted NPV |
|-----------------|-----------------------|--------------------------|-------------------------|----------------------|---------|----------|--------------|--------------|
| years | °C | | m | % | \$/W | \$/W | \$/W | |
| 5 | 40 | 800 | 0.5604 | 1.46 | 0.196 | 0.415 | 0.611 | 0.630 |
| 10 | 40 | 650 | 0.6435 | 1.58 | 0.206 | 0.540 | 0.746 | 1.409 |
| 15 | 40 | 650 | 0.7066 | 1.62 | 0.210 | 0.581 | 0.791 | 1.905 |

Table 1: Systems optimized for differing lifespan. Discount rate of 0.1, operating cost rate of 0.05.

Table 2 compares the effects of electricity price on the system. Commercial and industrial users may value electricity differently, and electricity prices differ greatly from state to state.

| Price of Electricity | Oil Inlet Temperature | Flue Gas Reynolds Number | Heat Exchanger Depth, L | First Law Efficiency | TE Cost | Hex Cost | Overall Cost | Weighted NPV |
|----------------------|-----------------------|--------------------------|-------------------------|----------------------|---------|----------|--------------|--------------|
| \$/kW-hr | °C | | m | | \$/W | \$/W | \$/W | |
| 0.10 | 40 | 650 | 0.6435 | 1.58 | 0.206 | 0.5401 | 0.746 | 1.409 |
| 0.05 | 40 | 900 | 0.5149 | 1.38 | 0.189 | 0.3586 | 0.5481 | 0.510 |
| 0.03 | 40 | 1050 | 0.3187 | 1.09 | 0.162 | 0.2409 | 0.4032 | 0.207 |

Table 2: Systems utilizing different sale prices of electricity. Lifespan of 10 years, discount rate of 0.1, operating cost rate of 0.05.

Table 3, found on the next page, compares systems evaluated using discount rates of 0.1, 0.15, and 0.2.

| Discount Rate | Oil Inlet Temperature | Flue Gas Reynolds Number | Heat Exchanger Depth, L | First Law Efficiency | TE Cost | Hex Cost | Overall Cost | Weighted NPV |
|---------------|-----------------------|--------------------------|-------------------------|----------------------|---------|----------|--------------|--------------|
| | °C | | m | | \$/W | \$/W | \$/W | |
| 0.1 | 40 | 650 | 0.6435 | 1.58 | 0.206 | 0.540 | 0.746 | 1.409 |
| 0.15 | 40 | 700 | 0.5972 | 1.53 | 0.201 | 0.481 | 0.682 | 1.086 |
| 0.2 | 40 | 750 | 0.5467 | 1.47 | 0.196 | 0.428 | 0.623 | 0.852 |

Table 3: Systems evaluated using different discount rates. Price of electricity is \$0.10/kWhr, lifespan of 10 years, operating cost rate of 0.05.

The next two tables explore special cases. Table 4 contains the parameters of a worst case simulation. The price of electricity used was \$0.03/kW-hr, the discount rate was 0.2, the operating cost rate was 0.15, and the lifespan of the system was 5 years.

| Oil Inlet Temperature | Flue Gas Reynolds Number | Heat Exchanger Depth, L | First Law Efficiency | TE Cost | Hex Cost | Overall Cost | Weighted NPV |
|-----------------------|--------------------------|-------------------------|----------------------|---------|----------|--------------|--------------|
| °C | | m | | \$/W | \$/W | \$/W | |
| 45 | 1450 | 0.1031 | 0.43 | 0.1203 | 0.1435 | 0.2637 | 0.0173 |

Table 4: A worst case system with lifespan of 5 years, electricity price of \$0.03/kWhr, a discount rate of 0.2, and an operating cost rate of 0.15.

Table 5 contains optimized parameters for a system using a hypothetical \$15,000 per cubic meter heat exchanger. All previous simulations used a heat exchanger price of \$7500 per cubic meter. The price of electricity used was \$0.10/kW-hr, the discount rate was 0.1, the operating cost rate was 0.05, and the lifespan of the system was 10 years.

| Heat Exchanger Cost | Oil Inlet Temperature | Flue Gas Reynolds Number | Heat Exchanger Depth, L | First Law Efficiency | TE Cost | Hex Cost | Overall Cost | Weighted NPV |
|---------------------|-----------------------|--------------------------|-------------------------|----------------------|---------|----------|--------------|--------------|
| \$/m ³ | °C | | m | | \$/W | \$/W | \$/W | |
| 7500 | 40 | 650 | 0.6435 | 1.58 | 0.206 | 0.540 | 0.746 | 1.409 |
| 15000 | 40 | 850 | 0.504 | 1.39 | 0.189 | 0.735 | 0.925 | 1.132 |

Table 5: A system utilizing a heat exchanger design of twice the unit cost as previous simulations. Electricity price is \$0.1/kWhr, discount rate is 0.1, lifespan is 10 years, and operating cost rate is 0.05.

The final table examines the operating parameters of the heat exchanger for the lifetime and electricity price cases detailed in Tables 1 and 2. For all cases the discount rate was 0.1 and the operating cost rate was 0.05.

| System Lifespan | Price of Electricity | Oil Inlet | Oil Outlet | Air Inlet | Air Outlet | C* | Power Density | Exergy Ratio | Blower Power |
|-----------------|----------------------|-----------|------------|-----------|------------|------|-------------------|--------------|--------------|
| years | \$/kW-hr | °C | °C | °C | °C | | kW/m ³ | | |
| 5 | 0.10 | 40 | 130.18 | 150 | 64.33 | 0.95 | 18.08 | 0.633 | 0.138 |
| 10 | 0.10 | 40 | 133.85 | 150 | 60.85 | 0.95 | 13.89 | 0.687 | 0.109 |
| 15 | 0.10 | 40 | 135.26 | 150 | 59.50 | 0.95 | 12.90 | 0.700 | 0.119 |
| 10 | 0.03 | 40 | 115.78 | 150 | 78.01 | 0.95 | 31.13 | 0.472 | 0.134 |
| 10 | 0.05 | 40 | 127.75 | 150 | 66.64 | 0.95 | 20.91 | 0.597 | 0.158 |
| 10 | 0.10 | 40 | 133.85 | 150 | 60.85 | 0.95 | 13.89 | 0.687 | 0.109 |

Table 6: Operating parameters for the system lifespan and electricity price cases from Tables 1 and 2. Inlet and outlet temperatures were from the flue gas to oil heat exchanger.

The data contained in the tables above relies on a specific heat exchanger design operating at a specific set of parameters. To explore how an optimized design would behave under daily fluctuations in oil and flue gas flowrate, a single design with set parameters was

exposed to different values of C^* . Figures 4-7 plot the response of the first heat exchanger specified in Table 6 to changes in C^* .

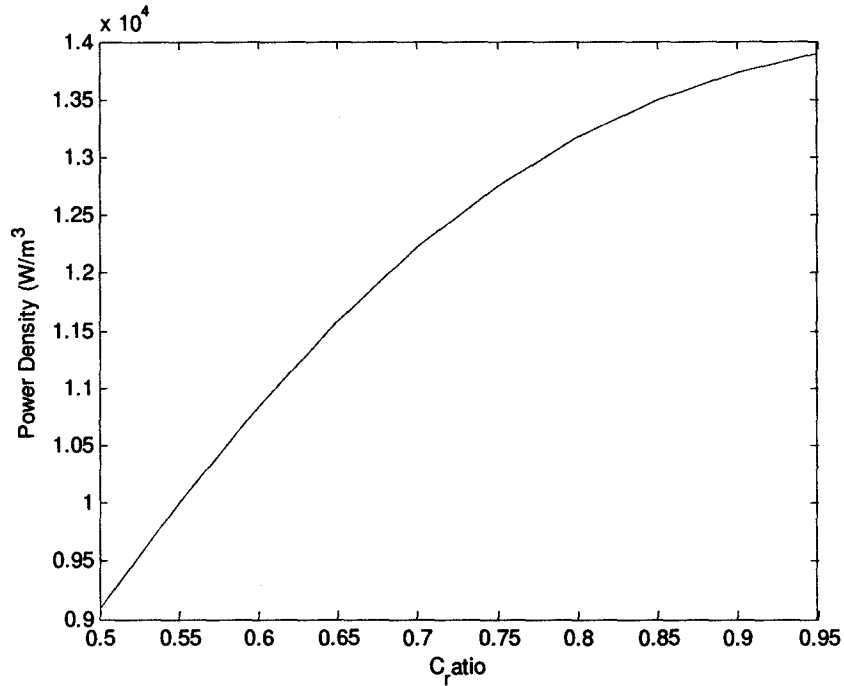


Figure 4: Power density as a function of C^* for a fully specified heat exchanger.

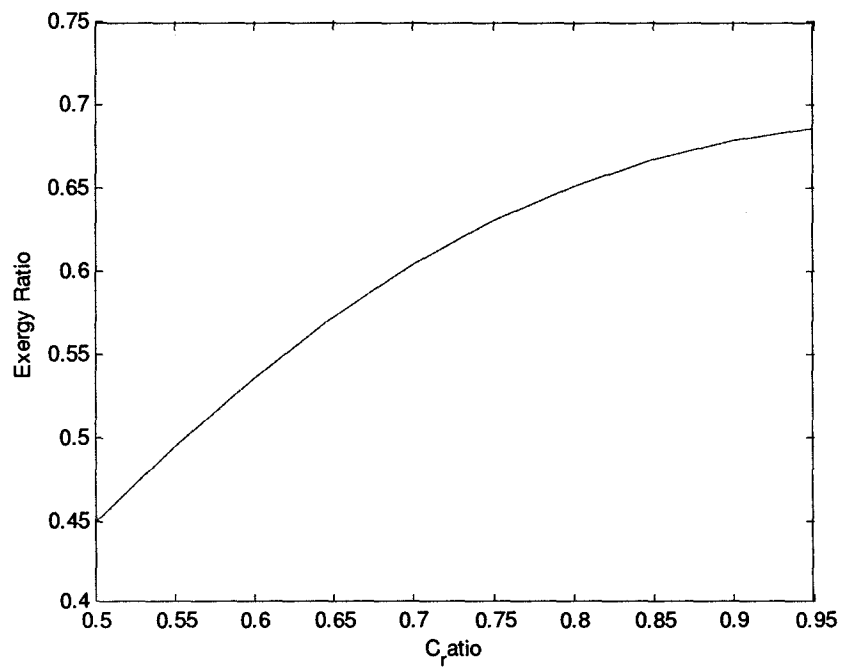


Figure 5: Exergy ratio as a function of C^* for a fully specified heat exchanger.

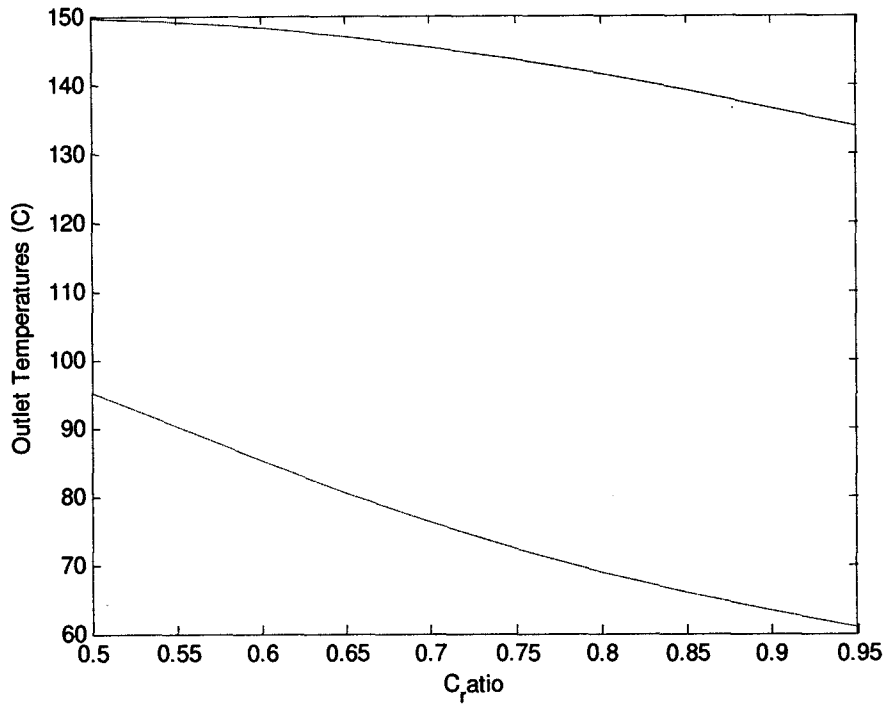


Figure 6: Temperatures of the oil outlet stream (upper line) and air outlet stream (lower line) as functions of C^* for a fully specified heat exchanger.

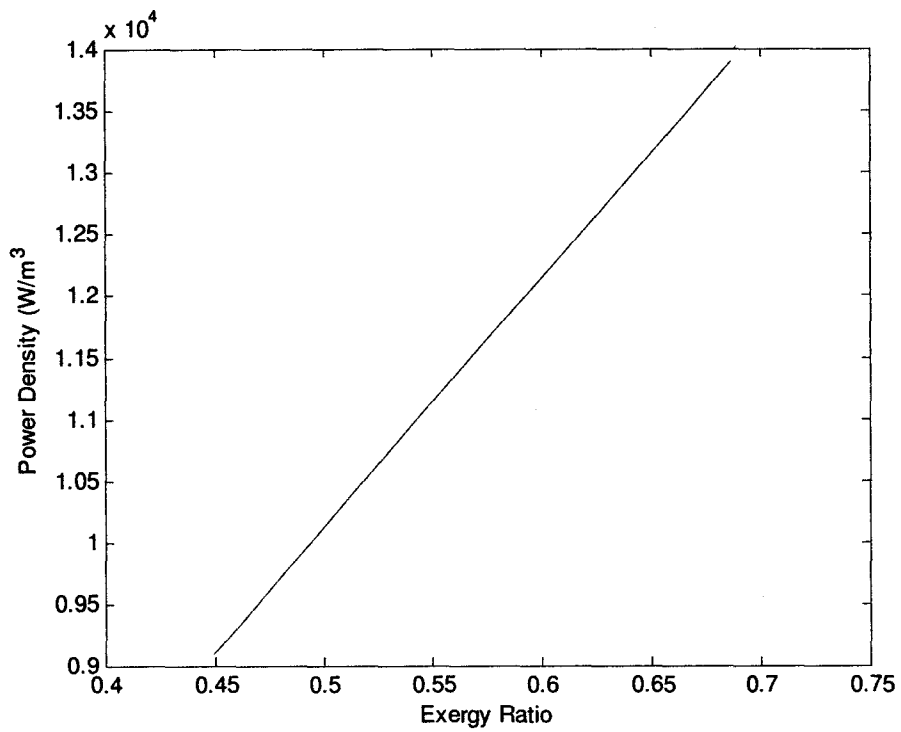


Figure 7: Power density as a function of exergy ratio in a fully specified heat exchanger, found by varying C^* .

5. Discussion

The model successfully optimized designs of the flue gas to oil heat exchanger while producing positive net present value using thermoelectric material of ZT value 0.8. A number of interesting correlations emerged that could help guide flue gas TEG system designers in the future.

All optimized systems favored 40° C oil inlet temperatures and C^* values greater than 0.95, as shown in Tables 1-6 and figures 4 and 5. It is obvious from Equation 19 that large temperature differentials and unity C^* result in high exergy ratios, thus resulting in high a volume of produced electricity. Additionally, system efficiency was inversely proportional to Reynolds number. This also is understandable given that pressure loss and thus pumping power increase with Reynolds number.

Figure 3 and Table 6 show that high heat exchanger power densities and high exergy ratios do not occur together. This is somewhat intuitive in that high exergy ratios, those on the order of 0.6-0.75, require large surface areas for high heat transfer to the thermal oil. As the heat exchanger grows, its volume increases and its power density decreases. The most effective systems from an exergy standpoint had power densities near 15 kW/m³. Conversely, high power densities, in this case those upwards of 70 kW/m³, were achieved by infinitely thin heat exchangers that only captured a small portion of the heat in the flue gas stream, resulting in exergy ratios near 0.05. Thus the model was tasked with balancing the emphasis on power density or exergy ratio in order to maximize profit.

The lifespan of the system plays a significant role in the design choices the model makes. Table 1 shows that the NPV of the fifteen year system is three times the NPV of the five year system. It is also apparent that larger heat exchangers and thus higher exergy rates

are more favorable in the long term, as the fifteen year system had a flow length of 0.7 m and an exergy ratio of 0.700 while the five year system had a flow length of 0.56 m long and an exergy ratio of 0.633. The role of the initial cost of the system is minimized by the extra electricity generated over time. Since the lifespan of neither the heat exchanger nor the TEG stack is currently known, it is reassuring to know that systems with short lifespan are still economically valuable.

The price of the electricity produced also significantly effects heat exchanger size, as seen in Table 2. As the value of the electricity produced decreases, so too does the thickness of the heat exchanger. A price drop of \$0.05 per kW-hr corresponded to a 0.13 m shortening of the heat exchanger flow length. The power density of the \$0.03 per kW-hr system was 31.13 kW/m^3 , or more than double the power density of the \$0.10 per kW-hr system.

Electricity price is a relevant parameter because it varies regionally, but also because an electricity wholesaler who uses the system will value electricity much lower than an industrial consumer who is using the system to reduce his electricity consumption. A utility would prefer a high power density but low initial cost system, whereas an industrial or commercial user would prefer a larger, more efficient system that can generate more electricity per unit of flue gas.

Table 3 and shows the effect of discount rate on the design of the system. High discount rates have the same effect as low electricity prices because they decrease the value of future cash flows. Thus, as discount rate increases, the value of the project decreases and lower initial cost systems become more favorable. The same result is seen when the operating cost rate is increased, as shown in Table 4, however the effect is much smaller.

To explore the limits of the model, two extreme cases were optimized and together they created a strong argument for the feasibility of a TEG system. The first case, detailed in Table 5, used the extreme values for lifespan, discount rate, operating cost rate, and electricity price used in previous optimizations, but the model was still able to generate a design with a positive NPV of 0.017, or roughly 1% of the NPV of the more realistic systems. The second case, shown in Table 6, was optimized using the base system parameters but with a doubled cost per volume of the heat exchanger. The model compensated for the high heat exchanger cost by slightly shrinking the depth of the heat exchanger. The resulting NPV of 1.132 was competitive with more conservatively priced designs, however the cost per watt of \$0.96 was almost \$0.20 higher than other designs.

Overall, the model was able to generate positive NPV systems despite a range of reasonable and extreme values for lifespan, operating cost rate, discount rate, and price of electricity. All systems modeled had a cost per watt between \$0.26 and \$0.96, values which are comparable to a number of renewable technologies. For firms not versed in the NPV method, a low cost per watt may be an important selling point.

Future work will involve including costs of the ancillary system equipment, including the blowers, oil pumps, ducting, and electricity conditioning hardware required for a complete system. Additionally, heat exchanger design firms should be employed to minimize the cost of the heat exchanger, as currently the heat exchanger accounts for more than 65% of the initial system cost in most designs.

The system appears promising and will only become more feasible as the quality and efficiency of thermoelectric materials continues to increase. However, significant challenges lay ahead before a commercial system can be put in place. One of the largest tasks is the

design of a robust TE heat exchanger. Currently no easy commercial solution exists, and the durability of research systems, including the porous copper systems being explored in Prof. Gang Chen's lab, is largely untested.

Overall the model and optimization strategy outlined in this paper demonstrated that a TEG based flue gas waste heat to electricity system, as it is was herein defined, is not only economically feasible, but also beneficial to a firm that installs it under the NPV capital budgeting criteria. The model produced value adding designs based on a wide range of time and budgeting constraints. Further work, in the form of modeling and real-world experimentation, should confirm the findings and assumptions in the study and hopefully lead to commercially available systems.

Acknowledgements

I'd like to thank Professor Gang Chen for supervising my project and giving me the chance to work in his lab. I'd also like to thank Andrew Muto for the opportunity to work on this project and his guidance during the entire process. There is absolutely no way I could have completed this project without his help.

Appendix A

Table 9-4 Surface Geometry, Flow Normal to Banks of Finned Tubes

(a) Circular tubes, circular fins

| Surface designation | Tube arrangement | Tube diameter | | Fin outside diameter | | Transverse tube spacing | | Longitudinal tube spacing | | Fins/in | Hydraulic diameter $4r_h$ | | Fin thickness δ | | Free-flow/ frontal area σ | Heat transfer area/ total volume α | | Fin area/ total area |
|---------------------|------------------|---------------|-------------|----------------------|-------------|-------------------------|-------------|---------------------------|-------------|---------|---------------------------|-------------|------------------------|-------------|----------------------------------|---|-------------------------|----------------------|
| | | in | 10^{-3} m | in | 10^{-3} m | in | 10^{-3} m | in | 10^{-3} m | | ft | 10^{-3} m | in | 10^{-3} m | | ft^2/ft^3 | m^2/m^3 | |
| | | | | | | | | | | | | | | | | | | |
| CF-7.34 | Staggered | 0.38 | 9.65 | 0.92 | 23.4 | 0.975 | 24.8 | 0.800 | 20.3 | 7.34 | 0.0154 | 4.75 | 0.018 | 0.46 | 0.538 | 140 | 459 | 0.892 |
| CF-8.72 | Staggered | 0.38 | 9.65 | 0.92 | 23.4 | 0.975 | 24.8 | 0.800 | 20.3 | 8.72 | 0.01288 | 5.95 | 0.018 | 0.46 | 0.524 | 163 | 535 | 0.910 |
| CF-8.72(c) | Staggered | 0.42 | 10.67 | 0.861 | 21.9 | 0.975 | 24.8 | 0.800 | 20.3 | 8.72 | 0.01452 | 4.43 | 0.019 | 0.48 | 0.494 | 136 | 446 | 0.876 |
| CF-11.46 | Staggered | 0.38 | 9.65 | 0.92 | 23.4 | 0.975 | 24.8 | 0.800 | 20.3 | 11.46 | 0.00976 | 2.98 | 0.016 | 0.41 | 0.510 | 209 | 686 | 0.931 |
| CF-7.0-1j | Staggered | 0.645 | 16.38 | 1.121 | 28.5 | 1.232 | 31.5 | 1.35 | 34.3 | 7.0 | 0.0219 | 6.68 | 0.010 | 0.25 | 0.449 | 82 | 269 | 0.830 |
| CF-8.7-1j(a) | Staggered | 0.645 | 16.38 | 1.121 | 28.5 | 1.232 | 31.5 | 1.35 | 34.3 | 8.7 | 0.01797 | 5.48 | 0.010 | 0.25 | 0.449 | 98.7 | 324 | 0.862 |
| CF-8.7-1j(b) | Staggered | 0.645 | 16.38 | 1.121 | 28.5 | 1.848 | 46.9 | 1.35 | 34.3 | 8.7 | 0.385 | 11.67 | 0.010 | 0.25 | 0.628 | 65.7 | 216 | 0.862 |
| CF-9.05-1j(a) | Staggered | 0.774 | 19.66 | 1.463 | 37.2 | 1.557 | 39.5 | 1.75 | 44.5 | 9.05 | 0.01681 | 5.13 | 0.012 | 0.31 | 0.455 | 108 | 354 | 0.835 |
| CF-9.05-1j(b) | Staggered | 0.774 | 19.66 | 1.463 | 37.2 | 1.982 | 50.3 | 1.75 | 44.5 | 9.05 | 0.02885 | 8.18 | 0.012 | 0.31 | 0.572 | 85.1 | 279 | 0.835 |
| CF-9.05-1j(c) | Staggered | 0.774 | 19.66 | 1.463 | 37.2 | 2.725 | 69.2 | 1.75 | 44.5 | 9.05 | 0.0445 | 13.59 | 0.012 | 0.31 | 0.688 | 61.9 | 203 | 0.835 |
| CF-9.05-1j(d) | Staggered | 0.774 | 19.66 | 1.463 | 37.2 | 2.725 | 69.2 | 0.80 | 26.3 | 9.05 | 0.01587 | 4.85 | 0.012 | 0.31 | 0.537 | 135 | 443 | 0.835 |
| CF-9.05-1j(e) | Staggered | 0.774 | 19.66 | 1.463 | 37.2 | 1.982 | 50.3 | 1.375 | 54.9 | 9.05 | 0.02108 | 6.43 | 0.012 | 0.31 | 0.572 | 108 | 354 | 0.835 |
| CF-8.8-1.0-j(a) | Staggered | 1.024 | 26.0 | 1.737 | 44.1 | 1.959 | 49.8 | 2.063 | 52.4 | 8.8 | 0.01927 | 5.89 | 0.012 | 0.31 | 0.436 | 91.2 | 299 | 0.825 |
| CF-8.8-1.0-j(b) | Staggered | 1.024 | 26.0 | 1.737 | 44.1 | 3.079 | 78.2 | 2.063 | 52.4 | 8.8 | 0.0443 | 13.21 | 0.012 | 0.31 | 0.642 | 58.1 | 191 | 0.825 |

Figure A-1: Dimensions of circular finned-tube surfaces, from Kays and London.

(b) Circular tubes, continuous fins

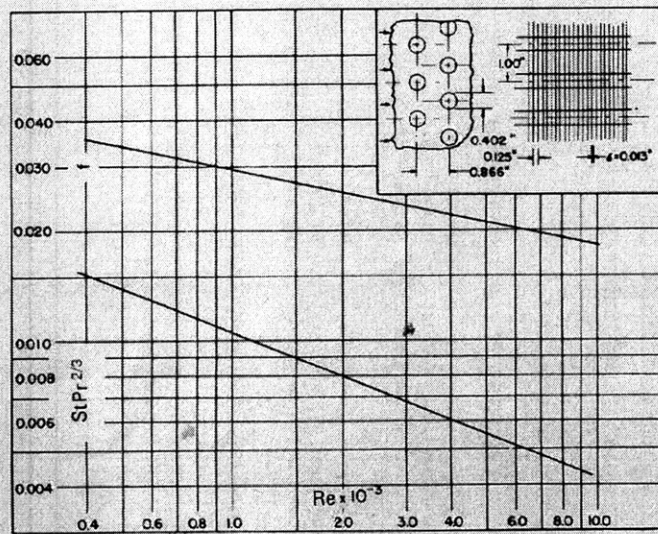
| Surface designation | Tube arrangement | Tube diameter | | Fin type | Fins/in | Hydraulic diameter, $4r_h$ | | Fin thickness δ | | Free-flow/ frontal area σ | Heat transfer area/ total volume α | | Fin area/ total area |
|---------------------|------------------|---------------|-------------|----------|---------|----------------------------|-------------|------------------------|-------------|----------------------------------|---|-------------------------|----------------------|
| | | in | 10^{-3} m | | | ft | 10^{-3} m | in | 10^{-3} m | | ft^2/ft^3 | m^2/m^3 | |
| | | | | | | | | | | | | | |
| 8.0-1T | Staggered | 0.402 | 10.21 | Plain | 8.0 | 0.01192 | 3.69 | 0.013 | 0.33 | 0.534 | 179 | 587 | 0.913 |
| 7.75-1T | Staggered | 0.676 | 17.17 | Plain | 7.75 | 0.0114 | 3.48 | 0.016 | 0.41 | 0.481 | 169 | 554 | 0.950 |

(c) Flat tubes, continuous fins

| Surface designation | Tube arrangement | Fin type | Tube length (parallel to flow) | | Tube width (normal to flow) | | Fins/in | Hydraulic diameter $4r_h$ | | Fin thickness δ | | Free flow/ frontal area σ | Heat transfer area/ total volume α | | Fin area/ total area |
|---------------------|------------------|----------|--------------------------------|-------------|-----------------------------|-------------|---------|---------------------------|-------------|------------------------|-------------|----------------------------------|---|-------------------------|----------------------|
| | | | in | 10^{-3} m | in | 10^{-3} m | | ft | 10^{-3} m | in | 10^{-3} m | | ft^2/ft^3 | m^2/m^3 | |
| | | | | | | | | | | | | | | | |
| 9.68-0.87 | In-line | Plain | 0.870 | 22.1 | 0.120 | 3.0 | 9.68 | 0.01180 | 3.60 | 0.004 | 0.102 | 0.697 | 229 | 751 | 0.795 |
| 9.1-0.737S | Staggered | Plain | 0.737 | 18.7 | 0.100 | 2.5 | 9.1 | 0.01380 | 4.21 | 0.004 | 0.102 | 0.788 | 224 | 735 | 0.813 |
| 9.68-0.87R | In-line | Ruffled | 0.870 | 22.1 | 0.120 | 3.0 | 9.68 | 0.01180 | 3.60 | 0.004 | 0.102 | 0.697 | 229 | 751 | 0.795 |
| 9.21-0.737SR | Staggered | Ruffled | 0.737 | 18.7 | 0.100 | 2.5 | 9.29 | 0.01352 | 4.12 | 0.004 | 0.102 | 0.788 | 228 | 748 | 0.814 |
| 11.35-0.737SR | Staggered | Ruffled | 0.737 | 18.7 | 0.100 | 2.5 | 11.32 | 0.01152 | 3.51 | 0.004 | 0.102 | 0.780 | 270 | 886 | 0.845 |

Figure A-2: Dimensions of continuous fin and flat tube finned-tube heat exchangers, from Kays and London.

Fig. 10-91 Finned circular tubes, surface 8.0-3/8T.



Tube outside diameter = 0.402 in = 10.2×10^{-3} m
 Fin pitch = 8.0 per in = 315 per m
 Flow passage hydraulic diameter, $4r_h$ = 0.01192 ft = 3.632×10^{-3} m
 Fin thickness = 0.013 in = 0.33×10^{-3} m
 Free-flow area/frontal area, σ = 0.534
 Heat transfer area/total volume, α = 179 ft²/ft³ = 587 m²/m³
 Fin area/total area = 0.913
 Note: Minimum free-flow area in spaces transverse to flow.

Figure A-3: Dimensions of surface 8.0-T, from Kays and London.

References

¹Engineering Scoping Study of Thermoelectric Generator Systems for Industrial Waste Heat Recovery, November 2006, US Department of Energy

²Turboden. "Waste Heat." < http://www.turboden.it/public/09Z00190_e.pdf > .February 21st, 2009.

³Electratherm. "50 kW Waste Heat Generator." <http://www.electratherm.com/pdf/50_kW_Cut_Sheet_Power_Tables_4152009.pdf>. March 14th, 2009.

⁴Rowe, D. M. Thermoelectrics Handbook Macro to Nano. Boca Raton, Fla: CRC Taylor & Francis, 2006.

⁵Incropera, Frank P., and Frank P. Incropera. Fundamentals of Heat and Mass Transfer. Hoboken, NJ: John Wiley, 2007.

⁶Kays, William Morrow, and A. L. London. Compact heat exchangers. New York: McGraw-Hill, 1984.

⁷Brealey, Richard A., Stewart C. Myers, and Franklin Allen. Principles of Corporate Finance. Boston: McGraw-Hill, 2006.